A Southern Hemisphere Wave Response to ENSO with Implications for Southern Africa Precipitation

KERRY H. COOK

Department of Earth and Atmospheric Sciences, Cornell University, Ithaca, New York

(Manuscript received 5 July 2000, in final form 12 December 2000)

ABSTRACT

Ensemble GCM simulations with an imposed, idealized warming of the eastern Pacific Ocean reveal two wave anomalies in the Southern Hemisphere, one in the eastern and one in the western hemisphere. Both are statistically significant at the 99% confidence level. Application of a steady-state linear model and a Rossby wave source analysis is used to diagnose the causes of the waves. The western hemisphere wave is forced by the advection and stretching of planetary vorticity by the divergent flow from the Southern Hemisphere component of the central Pacific ''twin anticyclones'' that straddle the equator during warm events. The eastern hemisphere wave is a result of the northeastward shift of the South Indian convergence zone (SICZ) that, in turn, is forced from the upper troposphere by convergence to the north. An upper-level convergence maximum over the equatorial Indian Ocean induces divergence to the south, encouraging vertical motion and precipitation to the northeast of the SICZ's normal position. The resulting anomalous upper-level convergence in the climatological position of the SICZ, as well as the anomalous vorticity flux convergence by the transients associated with an equatorward shift of the storm track behind the SICZ, force the eastern hemisphere Rossby wave.

Since a shift of the SICZ is a fairly robust observed consequence of ENSO events, these results suggest the mechanism by which drought conditions develop over southern Africa at the height of many warm events. Seasonal prediction capabilities in this region can be improved by monitoring and understanding the details and consequences of the adjustment of the Walker circulation near the equator outside of the Pacific Ocean basin.

1. Introduction

While ENSO has been associated with interannual variability in many regions, it has been challenging to identify the mechanisms of that influence. Inter-ENSO variability, the lack of precise measurements of atmospheric moisture, precipitation, and diabatic heating rates, and the relative shortness of the observing record all contribute to the difficulty.

Modeling has been used effectively to deepen our understanding of ENSO-related forcing of the global system. These modeling studies can be roughly sorted into two categories. First is simulations designed to study the response to steady tropical forcing, and includes work by Hoskins and Karoly (1981), Blackmon et al. (1983), Geisler et al. (1985), and Branstator (1990), to name only a small sample of the papers that have contributed to our basic understanding. This approach often provides a clearly identifiable response in the model, and the opportunity for deep analysis, but no information about the response in the context of natural or background variability.

Corresponding author address: Dr. Kerry H. Cook, Dept. of Earth and Atmospheric Sciences, Cornell University, 3114 Snee Hall, Ithaca, NY 14853.
E-mail: khc6@cornell.edu

The second category is modeling studies that use realistic ENSO events to force the model, such as the work of Lau and Nath (1990) and Hoerling and Ting (1994). Evaluation of this type of model experiment can include statistical significance if a large number of events are simulated, but the isolation of physical mechanisms is hampered by the complexity of the ENSO signal over time (inter-ENSO variability), just as in the observational record. In addition, other sources of variability that derive from the SST distribution and other sources are present, and these may obscure the ENSO-induced signal.

We began to wonder if a slightly different approach to modeling the global response to ENSO warm events might be useful for revealing the mechanisms of the global response. As described in section 3, we constructed a simple, time-dependent ENSO SST anomaly (SSTA) by examining pre-1990 warm events. This ENSO SSTA was imposed in twenty 16-month model integrations, each with different initial conditions, to produce 20 identical ENSO events and the opportunity to calculate significance statistics in the absence of inter-ENSO variability. By imposing climatological, seasonally varying surface features such as SSTs, albedo, and soil moisture, non-ENSO sources of year-to-year variations in the atmosphere were suppressed.

The global response of the precipitation field in these simulations is of particular interest, since most of the human impact of ENSO events is delivered through the modification of rainfall. A statistically significant precipitation signal due to the imposed warm event emerged at the 95% level and above in only a few regions in the model. The signal over the central Pacific, for example, is realistic and strong. More interestingly, the response in the southern Africa precipitation is nearly as strong as the central Pacific response, with a perturbation that is very similar to the observed response to warm events in that region. This is the first time, to my knowledge, that GCM simulations have captured the southern Africa precipitation signal associated with warm events.

Cook (2000) analyzes this southern African precipitation signal and relates it to the movement of the South Indian convergence zone (SICZ) and the presence of a wave response in the upper troposphere of the eastern hemisphere. This paper is focused on how that wave response and another statistically significant wave anomaly in the western part of the Southern Hemisphere come about.

The following section provides background on the Southern Hemisphere summertime precipitation response to warm events and reviews ideas about the global teleconnection of the ENSO signal. The GCM ensemble simulations and the linear model used to diagnose the wave response in the GCM are described in section 3. In section 4, the Southern Hemisphere wave response to ENSO SSTAs in the model is identified and, in section 5, the effect of the wave response on precipitation is analyzed through the column moisture budget. The cause of the Southern Hemisphere wave response is investigated in section 6 using a linear model analysis and vorticity budget diagnosis. Section 7 contains a summary and conclusions.

2. Background

a. Teleconnection of the ENSO Signal

The presence of a warm or cold event in the eastern Pacific can be communicated throughout the Tropics by a readjustment of the Walker circulation. During a warm event, the locations of the SST and convection maxima are displaced farther east in the Pacific Ocean and the up-branch of the Walker circulation moves to the east as well. This leads to anomalous divergence in the upper tropical troposphere over the central equatorial Pacific and, generally, anomalous convergence over the far western Pacific. The modification of the Walker circulation across the Pacific can induce changes in the atmosphere circulation over the Indian and Atlantic Ocean basins as well. This can occur either by purely atmospheric mechanisms (such as changed pressure gradients due to the Pacific response) and/or by the effects of changes wind stress on SSTs in the Indian and Atlantic Oceans (Latif and Barnett 1995).

The mean meridional (Hadley) circulation intensifies during warm events. The enhanced Hadley circulation is accompanied by increased zonal mean easterly flow aloft at low latitudes and stronger subtropical westerly jets (e.g., Horel and Wallace 1981) and an equatorward shift of the storm tracks in both hemispheres (Sinclair et al. 1997).

The ENSO signal is, of course, also present outside of the Tropics. One way this is thought to occur is through the generation of Rossby wave anomalies. Sardeshmukh and Hoskins (1985) and Rasmussen and Mo (1993) used evaluations of the tropical vorticity budget to identify anomalous Rossby wave sources associated with the 1982/83 and 1986/87 warm events, respectively. In simplified form, with vertical advection, tilting, and twisting neglected,[1] the vorticity equation can be written

$$\frac{\partial(\zeta + f)}{\partial t} + \mathbf{v}_\psi \cdot \nabla(\zeta + f) = -\mathbf{v}_\chi \cdot \nabla\zeta - v_\chi\beta - (\zeta + f)\nabla \cdot \mathbf{v}_\chi, \quad (1)$$

where ζ is relative vorticity, f is planetary vorticity, β is df/dy, and ∇ represents horizontal derivatives on a pressure surface. The horizontal velocity, has been written as the sum of its rotational, nondivergent part, ψ, and its irrotational, divergent part, χ. If the rhs of Eq. (1) is set equal to zero, the solution to the resulting equation is the classical Rossby wave. Thus, the terms on the rhs can be interpreted as a ''source term'' for Rossby waves, and each term can be computed and evaluated as a potential Rossby wave generator (Sardeshmukh and Hoskins 1988).

An analysis of Rossby wave sources requires a high quality dataset capable of providing the divergence field, and the product of the divergence and vorticity fields, with some accuracy. Sardeshmukh and Hoskins (1988) estimated Rossby wave sources for the 1982/83 warm event using archived European Centre for Medium-Range Weather Forecasts (ECMWF) forecasts. They found that nonlinear advection of absolute vorticity by the divergent flow,

$$\frac{\partial\zeta}{\partial t} \sim -\mathbf{v}_\chi \cdot \nabla(\zeta + f), \quad (2)$$

was important for determining the flow anomaly in the central tropical Pacific. Rasmussen and Mo (1993) analyzed the 1982/83 ENSO event in the National Meteorological Center (now the National Centers for Environmental Prediction) analysis, and suggested that the most prominent Rossby wave source is the planetary divergence term

[1] Sardeshmukh and Hoskins (1985), Rasmussen and Mo (1993), and the present analysis suggest that these terms are not of primary importance.

$$\frac{\partial \zeta}{\partial t} \sim -f\nabla \cdot \mathbf{v}. \quad (3)$$

This term maximizes in the subtropics since f increases with distance from the equator but the divergence anomaly decreases.

b. The Southern Hemisphere ENSO precipitation signal

During many, but not all, El Niño events, precipitation anomalies are negative over southern Africa south of 15°S, and positive to the northeast over northern Madagascar and Mozambique (e.g., Ropelewski and Halpert 1987; Janowiak 1988; Kiladis and Diaz 1989). This results in a southwest–northeast dipole pattern in interannual precipitation anomalies, a pattern that is also seen on seasonal and intraseasonal timescales. The southern Africa dipole was first described and related to ENSO by M. S. J. Harrison (Tyson 1986). Cook (2000) interprets the dipole precipitation pattern as a shift of the SICZ.

There is disagreement about the origin of the forcing that causes the southern Africa precipitation dipole response. Some studies implicate ENSO SSTAs directly, but other investigators suggest that the southern Africa precipitation field is strongly connected with the western Indian and Atlantic Oceans, and that the ENSO influence comes to southern Africa only through a forcing of Indian and/or Atlantic Ocean SSTs (Mason 1995; Nicholson and Kim 1997; Goddard and Graham 1999). Inter-ENSO variability, the presence of other important sources of variability on all timescales, the relative shortness of the observational record, and the complexity of the ocean environment near southern Africa (e.g., Rocha and Simmonds 1997) hamper a definitive analysis and make it difficult to identify the cause (or causes) of the precipitation dipole signal.

The GCM ensemble simulations presented here isolate a dipole precipitation signal in response to an ENSO warm event. We are able to identify the mechanism that operates in the model to produce the response. Our results suggest that the basic forcing for the southern Africa precipitation ENSO anomaly comes though the atmosphere alone and is not mediated by SSTAs in the Indian or Atlantic Oceans.

The relationships between ENSO and South American precipitation is weaker than the ENSO–southern Africa relationship, with the exception of the strong positive (negative) rainfall anomalies of Ecuador and northern Peru during warm (cold) events. There is a general tendency for reduced rainfall in the north and enhanced rainfall in the south during the austral summer of warm events (Ropelewski and Halpert 1987; Aceituno 1988; Kiladis and Diaz 1989), and drying in the north may extend southward into the central Andes Altiplano region. Lenters and Cook (1999) associate this reduced precipitation on the Altiplano with a cool, dry, southeasterly flow anomaly at low levels that stabilizes the atmospheric column. This flow anomaly is associated with enhanced frontal activity and a repositioning of the South Atlantic convergence zone, which brings wet conditions to the southeastern part of the South American continent (e.g., Gan and Rao 1991).

3. GCM simulations and linear model description

The atmospheric GCM is a version of the Geophysical Fluid Dynamics Laboratory Climate Dynamics Group model, with R30 horizontal resolution and 14 vertical sigma levels. The control simulation is a 20-yr integration with solar insolation, SSTs, soil moisture, cloud fraction, and land surface albedo changed seasonally, but the same for each of the 20 yr. Prescribed SSTs are from Shea et al. (1990), soil moisture values are from Mintz and Walker (1993), and the land surface albedo distribution is from Matthews (1984). The control climatology is formed by averaging individual months from a 20-yr integration of the model.

The December ENSO climatology is the average of monthly means from a 20-member ensemble set. Only December is analyzed here, since that month shows the strongest Southern Hemisphere wave response. Each member of the ensemble is a 15-month-long integration and has the same boundary conditions as the control integration except for a simple, time-dependent SST anomaly (described below). Initial conditions for the ensemble members are 20 ''snapshots'' of the atmospheric state from a perpetual-January integration of the same model with the same boundary conditions; the perpetual-January integration was started from an isothermal, dry, motionless atmosphere.

The imposed SSTAs represent an ENSO event with average SSTAs and warming confined to the eastern Pacific. They are Gaussian in shape and time dependent, with half-widths, magnitudes, and positions chosen by referring to observed warm events. The warming begins off the coast of South America in March of the first year and grows in extent and magnitude through November. The maximum anomaly is 2 K, which occurs on 15 November off the coast of Peru and Ecuador just south of the equator. The anomaly begins to weaken in December and continues to fade through March of the second year. Figures 1a,b show the imposed SSTAs for November and December of the first year of the integration.

The Student's t-test is used to assess confidence levels for differences between the control and ENSO climatologies. Because precipitation may be poorly represented by a Gaussian probability distribution function, the Mann–Whitney rank-sum test was also used to calculate the significance of the precipitation signal (von Storch and Zwiers 1999); the results were very similar to the Student's t-test results and only the Students, t results are presented here.

A linear model is used to associated wave structure

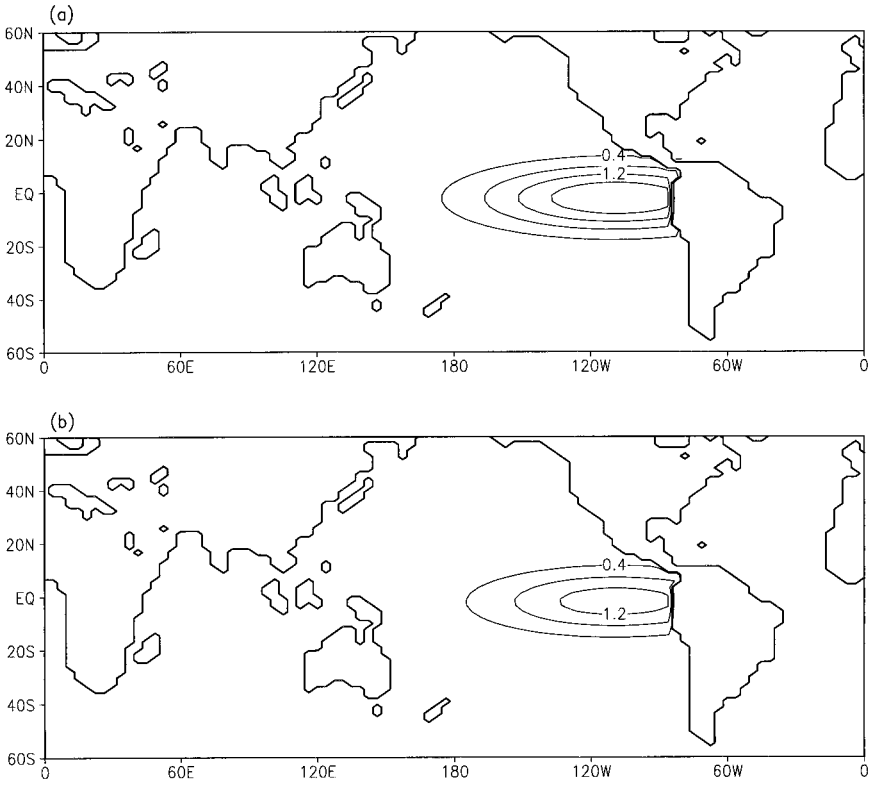

FIG. 1. (a) Nov and (b) Dec SST anomaly imposed in the GCM ensemble simulations. Contour intervals are 0.2 K, and continental outlines are shown as represented in the R3 GCM.

in the Southern Hemisphere with ENSO-induced modifications of the diabatic heating field, transient momentum and heat fluxes, and zonal mean basic state in the GCM. The linear model is governed by the linearized, steady-state primitive equations, with the same vertical sigma levels, horizontal resolution, and spectral representation as the GCM. [See Ting and Held (1990) for a detailed description of this model.] Here we either linearize the model about the zonal mean flow and temperature fields from the ENSO ensemble mean or the control climatology from the GCM.

Longitudinal structure in the linear model is generated by including three-dimensional diabatic heating fields (dry convective, sensible, radiative, and condensational heating), momentum (vorticity and divergence) and thermal transients, and topography. Each of these fields is taken from the GCM output, with the momentum and thermal transients calculated from the time-mean GCM output as residuals in the time-mean momentum and thermodynamics equations. By including these three-dimensional fields individually, or only in certain locations, linear model solutions are generated that associate stationary wave structure in the atmospheric flow and temperature fields with the distributions of heating, transient activity, and/or topography. Conclusions concerning cause and effect based on the linear model solutions are subject to interpretation since it is a steady-state model.[2]

4. Identification of the Southern Hemisphere wave response

Figure 2 shows the difference in the 171-hPa eddy streamfunction between the averages of the 20 GCM ENSO simulations for December and the 20 Decembers of the control climatology. Taking differences of the eddy fields, where ''eddy'' refers to the departure from the zonal mean, filters out the zonal mean response and leaves only the difference in the wave response. Shading in Fig. 2 indicates levels of confidence in the differences between the full (not eddy) streamfunction fields. Lighter shading shows where the full streamfunction in the ENSO simulation differs from the control at the 90%

[2] The three-dimensional heating, transients, and topography fields are sometimes referred to as ''forcing functions'' in the literature, but this terminology can be misleading. It is safe to think about topography as forcing atmospheric structure, but transients and heating distributions are themselves, in part, a response to the flow and temperature anomalies. Unless a well-defined chain of events can be hypothesized, it is best to think of the relationship between the transients and heating, and the linear solution, as a mutual adjustment with no implied time sequence.

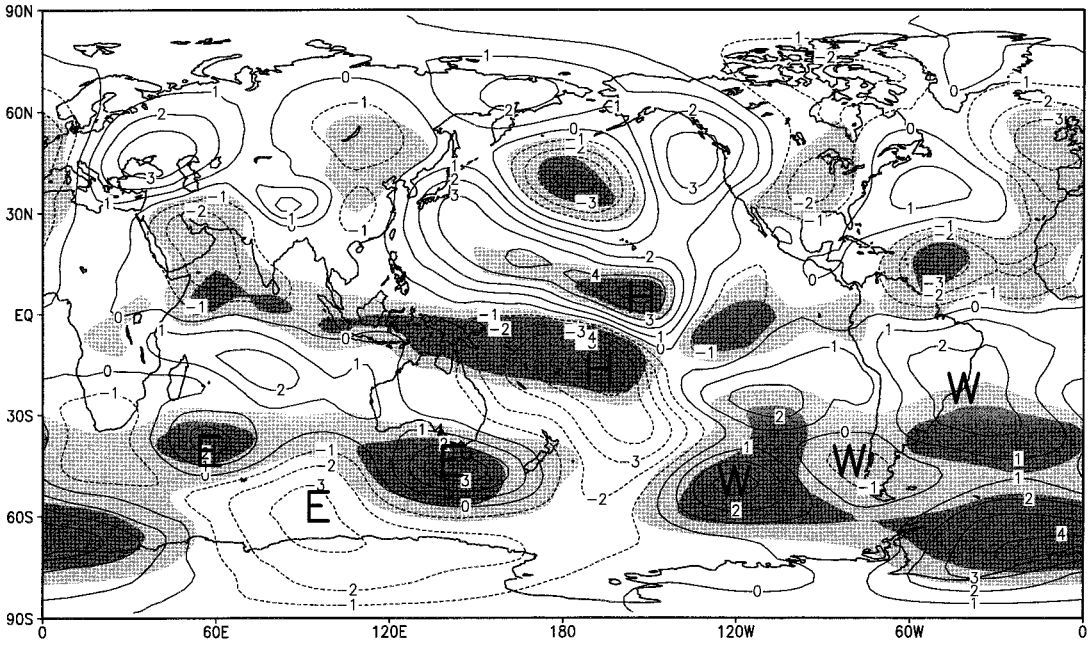

FIG. 2. Difference in the ensemble Dec eddy streamfunction at 171 hPa for ENSO minus control. Central Pacific anticylonic anomalies are marked with H's, and the two Southern Hemisphere wave trains are indicated by E's in the eastern hemisphere and W's in the western hemisphere. Contour interval is 10^6 m^2 s^{-1}. Lighter shading indicates that the differences between the full streamfunction fields are significant at the 90% level, and darker shading marks the 99% confidence regions.

confidence level; darker shading indicates the 99% confidence level.

The tropical response to eastern Pacific warming in the model includes a pair of anticyclonic streamfunction anomalies straddling the equator near 160°W. They are marked with H's in Fig. 2, and both are significant at the 99% level. The anticyclone pair is always observed during ENSO events (e.g., Arkin 1982) and reflects a weakening of the upper-level eddy cyclonic flow over the relatively cold eastern and central Pacific. When compared with the magnitudes of anticyclonic anomalies associated with ENSO events in the National Centers for Environmental Prediction–National Center for Atmospheric Research reanalysis (Kalnay et al. 1996), the streamfunction perturbation in the GCM is well placed but somewhat weak. In the model, the 1.8-K SSTAs of December are associated with streamfunction anomalies of 5–8 $\times$ 10^6 m^2 s^{-1}. In the reanalysis, for example during December 1986 when the SSTAs were below 1.5 K, the magnitudes of the upper-tropospheric streamfunction anomalies near 160°W longitude were over 8 $\times$ 10^6 m^2 s^{-1}. The strong ENSO event of 1997/98 generated December streamfunction anomalies greater than 18 $\times$ 10^6 s^{-1} in the Northern Hemisphere and 12 $\times$ 10^6 s^{-1} in the Southern, according to the reanalysis.

In the middle latitudes of both hemispheres there is a wavy response in the model (Fig. 2), with positive and negative anomalies of similar magnitudes alternating within the westerlies. In both hemispheres, wave structure in the GCM is more regular than is typically observed; this is at least partly due to the suppression of sources of variability in the model design. The Pacific–North America (PNA) pattern, marked by a strengthening of the Aleutian low and a wave train across North America to the east is in evidence; at lower levels (e.g., 700 hPa) the PNA is very similar to the observed PNA (Horel and Wallace 1981).

The Southern Hemisphere response is generally more highly significant than the Northern Hemisphere response. This occurs despite the fact that the winter hemisphere westerlies are more likely to support stronger wave activity, since the smaller background variability of summer hemisphere allows the signal from the modest ENSO warm event to emerge more clearly. Two wavelike patterns are generated in Southern Hemisphere subtropical and middle latitudes. One consists of the high–low–high pattern in the eastern hemisphere southeast of Africa (marked with E's in Fig. 2), and the other is the western hemisphere high–low–high pattern crossing South America (marked with W's). (The two Southern Hemisphere patterns are referred to here as ''waves'' for convenience, but we have not yet shown that the sequences of anomalies are physically connected.)

Figures 3a,b,c show modeled differences in eddy geopotential (ENSO minus control) at 171, 568, and 850 hPa, respectively, for the Southern Hemisphere. Shading indicates areas where the full geopotential in the ENSO simulation is significantly different from the control at

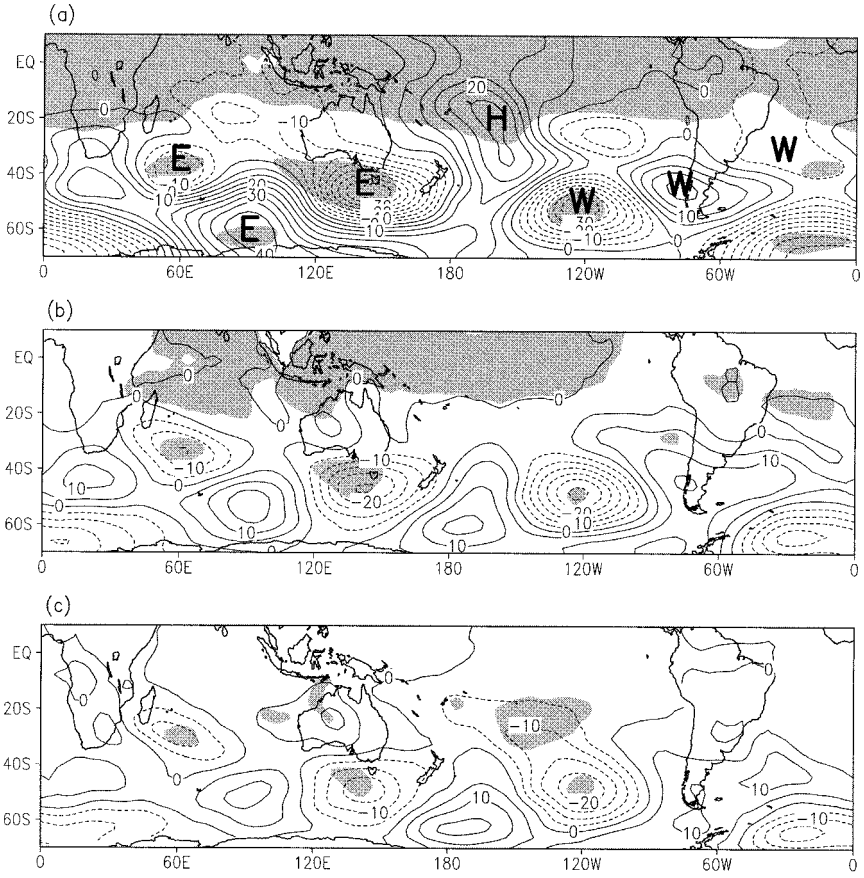

FIG. 3. Differences in Dec eddy geopotential in the Southern Hemisphere for ENSO minus control for the ensemble simulations at (a) 171, (b) 568, and (c) 866 hPa. Contour interval is 5 gpm. Shading indicates significance at the 99% level between the full geopotential fields. See text for definitions of H, E's, and W's.

the 99% confidence level. As indicated by the shading in Fig. 3a, the response in the upper tropical troposphere is highly significant at all latitudes. The zonal mean response (not shown) has positive height anomalies in the Tropics and lower heights in the subtropics, representing a strengthening of the Hadley circulation during warm events. Such a response is well known from modeling and observational studies (e.g., Oort and Yienger 1996; Roechner et al. 1996).

The Southern Hemisphere member of the anticyclone pair is marked with an H in Fig. 3a. The two Southern Hemisphere wave trains identified in the upper-level eddy streamfunction anomalies (Fig. 2) are clearly represented in the eddy geopotential (Fig. 3a); they are both statistically significant, but the eastern hemisphere wave (marked with E's) is more highly significant than the western hemisphere wave (marked with W's). The paths of the waves are similar to preferred propagation paths for Rossby waves in these regions (Hsu and Lin 1992; Hoskins and Ambrizzi 1993).

The wave anomalies persist through the middle and lower troposphere. The vertical structure of the eddy response in the Tropics, most notably, the upper-level anticyclone over the central Pacific, is baroclinic. The feature is not discernible at 568 hPa (Fig. 3b) and is manifest as a negative anomaly (cyclonic) near the surface (Fig. 3c). In contrast, the two Southern Hemisphere wave trains have barotropic structure, with the anomalies preserving their signs through the depth of the troposphere. Both the magnitudes and statistical significance of the perturbations become smaller at lower levels. The significance of the highs is diminished even in the middle troposphere (Fig. 3b). (The generally smaller significance of the highs as compared to the lows is probably due to the choice of the Student's t statistic. The symmetry of the Gaussian probability distribution function on which this statistic is based does not account for the fact that low pressure anomalies tend to have a greater magnitude than high pressure anomalies due to centrifugal accelerations.) Near the surface (Fig. 3c), the wave response over South America is poorly defined. The eastern hemisphere wave train, on the other hand, remains strong to the surface.

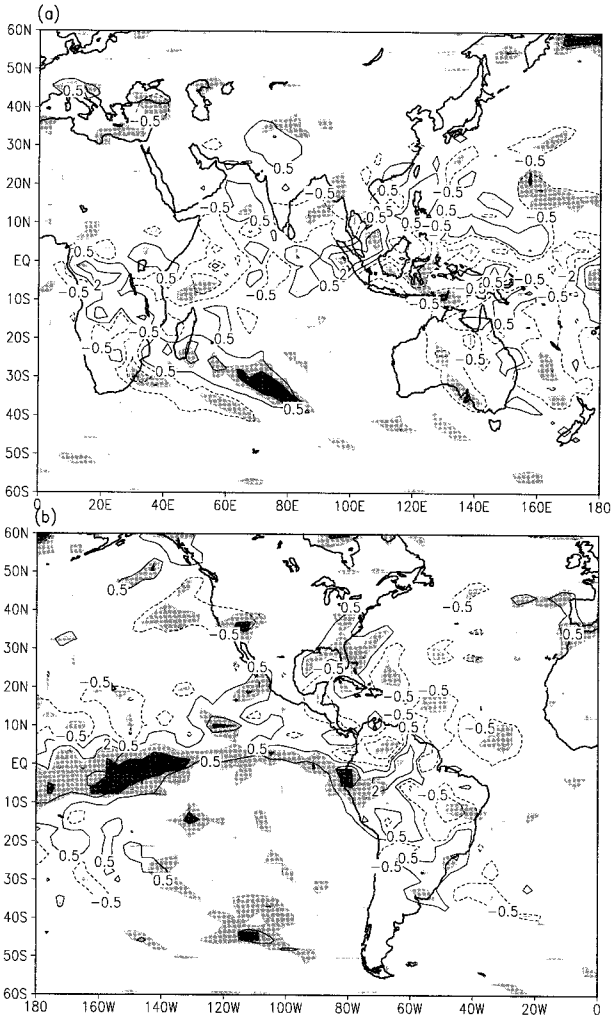

FIG. 4. Modeled precipitation differences in the (a) eastern hemisphere and (b) western hemisphere due to eastern Pacific warming in the ensemble simulations (ENSO minus control). Contour levels of −2.0, −0.5, 0.5, and 2.0 mm day^{-1} are plotted. Light shading indicates statistical significance at the 90% level, and dark shading at the 99% level.

5. Modeled Southern Hemisphere precipitation response

Figure 4a shows the difference between the modeled ENSO December precipitation climatology (the average of the 20 December means from the ENSO ensemble members) and the control (the average of the 20 December means) in the eastern hemisphere, and Fig. 4b shows the western hemisphere. Light shading indicates the 90% confidence level, and darker shading the 99% level.

As is observed during ENSO warm events, precipitation over the central equatorial Pacific Ocean is increased during the modeled event, with maximum increases over the surface temperature maximum, which occurs to the west of the SSTA maximum. This response is accurately captured in the model at a high level of significance.

The precipitation response southeast of Africa is also statistically significant. This southwest–northeast dipole signature is very similar in both structure and magnitude to the observed ENSO signal in this region (e.g., Kiladis and Diaz 1989). Decreases in rainfall of up to 4 mm day^{-1} are simulated over southeastern South Africa, with increases to the northeast. Enhanced precipitation rates of up to 2 mm day^{-1} occur over southern Mozambique on the east coast (25°S and 35°W), and stretch eastward over southern Madagascar and 30° of longitude farther southeast. Inland, over most of Zimbabwe (near 20°S and 30°W), for example, precipitation rates are lower in the ENSO simulation by about 0.5 mm day^{-1}.

Cook (2000) associates this dipole anomaly with a northeastward shift of the SICZ. The SICZ precipitation maximum is supported over land by low-level convergence in the moist environment, where the flow about the continental thermal low meets the flow about the South Indian Ocean (subtropical) high. The advection of moisture in the southwestern quadrant of the high is also important, especially for supporting the diagonal extension of the SICZ over the ocean to the southeast. The negative height anomalies at low levels associated with ENSO (Fig. 3c) weaken the western portion of the subtropical high, and the SICZ is shifted to the northeast. In the climatological location of the SICZ, rainfall is decreased, and this decrease is further supported by the anomalous onshore advection of dry air (Cook 2000). Therefore, understanding how the eastern hemisphere wave response comes about will allow us to physically connect the southern Africa precipitation signal with ENSO SSTAs.

Over South America, the precipitation response in the model is also fairly realistic. High precipitation rates over Ecuador and northern Peru are correctly simulated with high significance. Higher precipitation rates along the southeast coast and drier conditions to the north, for example, in the Amazon basin, are also associated with warm events in the literature (e.g., Aceituno 1988), but the connection with ENSO is not thought to be as robust as for southern Africa. Consistent with observational analyses, the model simulates lower significance for the South America response compared with the southern Africa response. Observational analyses suggest that the Altiplano (central Andes) region may be dry during warm events, but the model does not capture this signal.

Unlike the response over southern Africa, the precipitation perturbation over South America is not clearly related to the wave response. The western hemisphere wave does not penetrate to the lower troposphere as strongly as the eastern hemisphere wave (Fig. 3c), so the western hemisphere wave is less likely to influence the precipitation field. The circulation perturbation needs to reach below 750 hPa before it can perturb the moisture budget significantly, since most of the atmospheric column moisture is located at low levels. Only

the first downstream low, near 45°S and 120°W, penetrates to the surface with any strength (Fig. 3c). This low is coincident with a significant precipitation increase (Fig. 4b), but this is a region of extremely low climatological precipitation

6. Cause of the Southern Hemisphere waves

The previous section connects the precipitation perturbation over southern Africa with one of the Southern Hemisphere waves. Understanding the cause of the wave, therefore, will connect the precipitation perturbation with the SSTAs of the eastern Pacific. To make this connection, the linear model and vorticity budget diagnostics described in section 3 are used to understand how the wave responses are generated.

a. Linear model analysis

Before using the linear model to associate the Southern Hemisphere waves with individual factors, the degree to which linear stationary wave dynamics can reproduce the GCM wave response to ENSO is assessed. To do this, two ''full'' linear model solutions are calculated. One uses zonal mean fields from the control December climatology, as well as three-dimensional heating fields, transients, and topography from the control to generate zonal asymmetry in the model. The second uses zonal mean and three-dimensional fields from the ENSO December climatology.

The twin anticyclone anomalies in the linear solution are slightly stronger than their GCM counterparts and are located about 15° of latitude farther poleward (not shown). Both anomalies also extend farther east than in the GCM simulation. The anticyclones in the full linear solution actually resemble the observed anticyclones associated with warm events (e.g., for 1986/87) more closely than the GCM anticyclone perturbations. This could be spurious, or it could indicate that some nonlinear process in the GCM is overdamping the upper-level response in the tropical Pacific in the GCM.

The difference between the full linear solutions (ENSO minus control) is shown in Fig. 5a for the 171-hPa eddy geopotential in the Southern Hemisphere. Since the linear model solves for eddy fields, Fig. 5a is directly comparable to Fig. 3a. The linear solution is quite similar to the GCM in the eastern hemisphere and the central tropical Pacific. However, the wavy structure in the GCM's western hemisphere is poorly represented, perhaps being disrupted by the eastward extension of the central Pacific anticyclone.

This level of agreement between the GCM and linear model suggests that there is something to be learned from a linear model analysis, but with some reserve. The agreement between the linear and nonlinear (GCM) solutions is not as strong as in some other studies, especially those in midlatitudes. However, Ringler and Cook (1995) show that this type of model may be better suited for the Tropics. In the Tropics, structure in the diabatic heating field is more closely related to stationary wave structure than in middle latitudes, where mechanical forcing (flow obstruction) associated with topography is much more important. Several authors have shown that the purely linear formulation of the mechanical forcing is incorrect in many situations; the diabatic heating field is always correctly represented because it is simply imposed in the model. On the other hand, this study is concerned with global-scale responses that cross critical latitudes where the linear assumption become theoretically invalid and the model relies heavily on the parameterization of dissipation.

Figure 5b shows the difference in linear model solutions when only diabatic heating (condensational, radiative, plus sensible heat fluxes) is included. Both linear solutions used to generate Fig. 5b are linearized about the GCM's control basic state. Consistent with the results of Hoerling et al. (1995) for the Northern Hemisphere winter, differences in the zonal-mean basic state in the GCM do not influence the linear solutions in this case. The difference in the linear solutions associated with diabatic heating is essentially a wavenumber-1 perturbation confined between 10°N and 40°S, with an amplified response east of the three continents. There is no hint of the tropical anticyclone or the Southern Hemisphere midlatitude waves and, in fact, the responses east of Africa and South America are of opposite sign to those in the GCM (Fig. 3a) and the full linear solution (Fig. 5a).

The difference in the linear solutions consistent with the modification of the thermal transients during the warm event, shown in Fig. 5c, is also centered in the summer hemisphere subtropics, and it is weaker than the response to diabatic heating. It dampens the structure associated with diabatic heating over Australia and the southern Indian Ocean, and shifts the Bolivian high southward.

The difference in the linear solutions associated with differences in the convergence of transient vorticity fluxes is shown in Fig. 5d. Both Southern Hemisphere wave strains emerge clearly (compare with Fig. 3a). The magnitudes tend to be weaker than in the GCM, particularly in the western hemisphere, but the structure is very similar. A positive height anomaly is centered east of Australia, which superimposes destructively on the responses to diabatic heating (Fig. 5b) in the full solution (Fig. 5a). The response to vorticity transients also opposes the response to diabatic heating directly off the east coasts of southern Africa and South America.

All of the perturbations from the linear model are weaker in the lower troposphere (not shown). The wave structure consistent with diabatic heating is baroclinic in the eastern hemisphere subtropics, being proportional to the vertical derivative of the heating, so the positive perturbations off the southeast coast of Africa are aligned with negative perturbations near the surface. The association with thermal transients is relatively

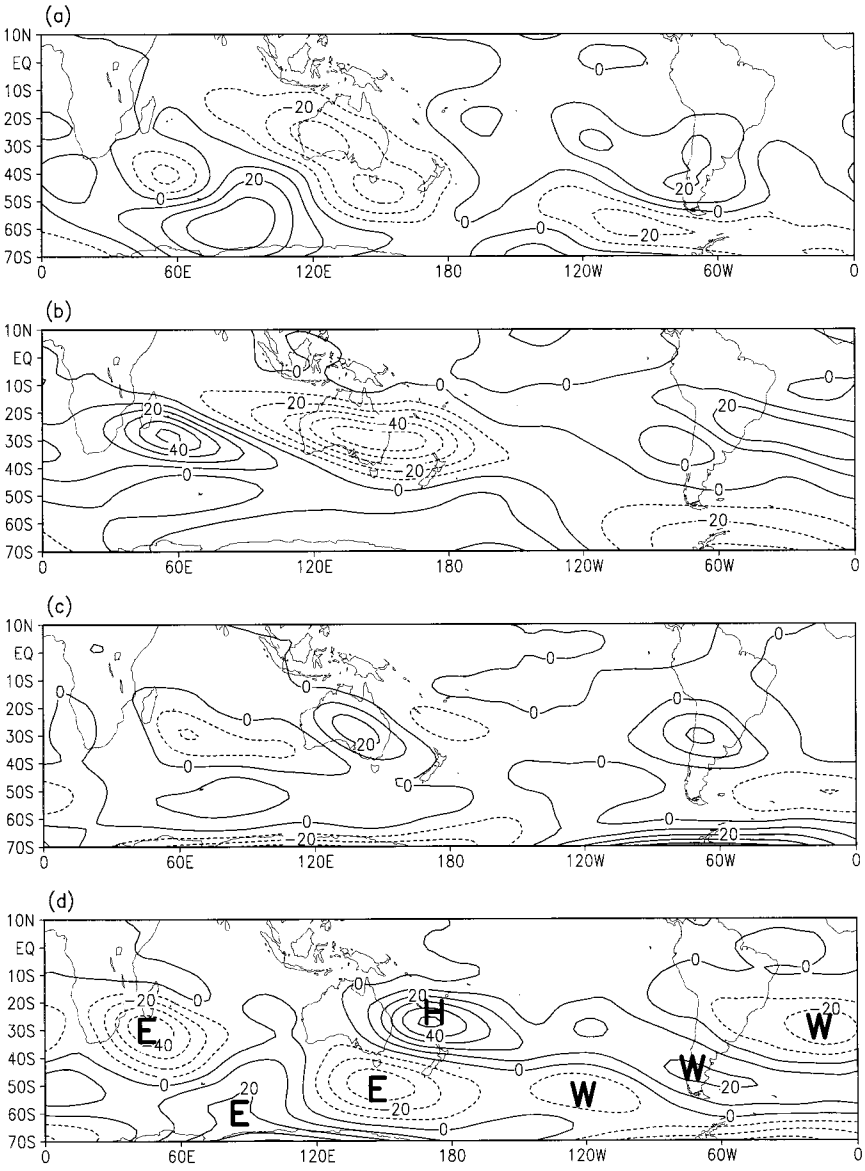

FIG. 5. Differences in linear solutions (ENSO minus control) for eddy geopotential at 171 hPa with (a) perturbed basic state and diabatic heating, topography, and transients; (b) control basic state and diabatic heating alone; (c) control basic state and thermal transients alone; and (d) control basic state and vorticity transients alone. Contour intervals are 10 gpm. In (d), H marks the Pacific anticylone anomaly, and the Southern Hemisphere waves are indicated by E's and W's as in Fig. 2.

more important at lower levels. Consistent with the discussion of Lau and Holopainen (1984), the wave structure associated with vorticity transients is equivalent barotropic.

The regionality of the connection between the wave anomalies and the vorticity transients is explored by including vorticity transients only in particular regions. This set of linear model solution shows that the eastern hemisphere wave is primarily associated with a modification of the vorticity transients over Africa, and that transients at all vertical levels are involved. The African vorticity transients are associated with some relatively minor remote effects, including negative eddy geopotential heights over subtropical South America, but they are not associated with the western hemisphere wave. Similarly, the western hemisphere wave anomaly is primarily associated with the modification of vorticity transients over South America alone.

Other studies have associated vorticity (momentum) transients with extratropical response to ENSO. For example, a case study of the 1982/83 event by Kok and Opsteegh (1985) and a model analysis by Held et al.

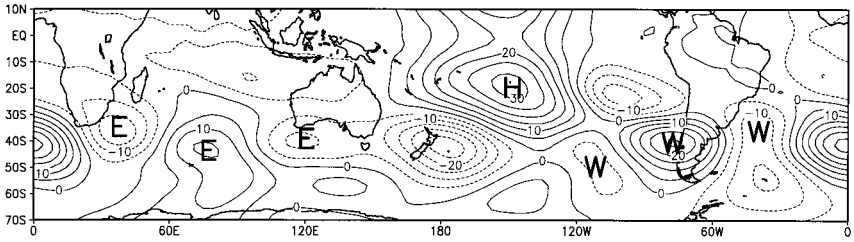

FIG. 6. Difference in 171-hPa eddy geopotential for ENSO minus control for the perpetual-Dec GCM simulations. Contour interval is 10 gpm; H marks the Pacific anticylone anomaly, and the Southern Hemisphere waves are indicated by E's and W's as in Fig. 2.

(1989) suggest important roles for the transients in determining the Northern Hemisphere midlatitude response to warm events. Hoerling and Ting (1994) connect an eastward extension of the Pacific storm track transients with the occurrence of the PNA pattern during warm events. They suggest that the positioning of a PNA response to ENSO is determined more by the longitudinal position of the storm track than by the longitudinal position of the tropical forcing.

The linear model analysis associates anomalous momentum convergence by the transients with the Southern Hemisphere wave anomalies, but fails to establish a cause-and-effect relationship between the wave anomalies and the modification of diabatic heating fields by the equatorial Pacific SSTAs. There are several possible interpretations of the linear model results. It could be that the vorticity transients are modified in some way that the linear model misses, due to being linearized about the zonal mean or due to some nonlinear process, and the modification of the transients causes the wave anomalies. Another possibility is that the waves are being more directly forced by some mechanism that the linear model misses, and the perturbation of the transients is a consequence of the wave anomalies. Additionally, the stationary wave anomalies and the modification of the transients may be independent, simultaneous responses to some other forcing. The Rossby wave source analysis that follows helps distinguish among these possible interpretations of the linear model results and relates the wave anomalies to the eastern Pacific forcing.

b. Rossby wave source analysis

To identify regions of Rossby wave forcing in the GCM ensemble simulations, each term in the rhs of Eq. (1) is calculated for each month of the ENSO and control climatologies. The difference is formed to locate regions in which the Rossby wave sources change due to the warm event and to understand the mechanisms of the changed sources.

There are two concerns about this analysis using the GCM ensemble simulation output. First, the time-mean fields are used since the Rossby wave source terms were not collected in the course of the GCM ensemble integrations. For example, the approximation

$$\overline{-\mathbf{v}_\chi \cdot \nabla \zeta} \approx -\mathbf{v}_\chi \cdot \nabla \overline{\zeta} \tag{4}$$

is used, where the overbars refer to the time average for a given month (an average of 20 December means). This approximation is worrisome because the linear model analysis shows that changes in transient activity are involved in the Southern Hemisphere wave perturbation and because the advection of transient relative vorticity by the time-dependent flow may be an important vorticity source near the equator (Sardeshmukh and Hoskins 1985).

The second concern is the potential for Rossby wave source terms to be noisy, especially those containing divergence and the product of the divergence and relative vorticity. Using the ensemble monthly means for December, an average is formed by averaging 620 days (20 ensemble members $\times$ 31 days). Flow, temperature, and even precipitation signals emerge clearly from such an average, especially when guided by the significance analysis, but the significance analysis is not available for the Rossby wave source terms. The observationally based analyses by Sardeshmukh and Hoskins (1985) and Rasmussen and Mo (1993), however, extracted useful information from much shorter time series.

Because of these concerns, two additional GCM integrations were performed to support and confirm the Rossby wave analysis of the ensemble simulations. These are 2000-day perpetual-December simulations, with boundary conditions identical to the 15 December boundary conditions of the ensembles. Initial conditions for both are an isothermal, dry atmosphere at rest, and the first 150 days of each integration are discarded as a spinup period. Climatologies are formed by averaging the remaining 1850 days of the integration.

Figure 6 shows the difference in the Southern Hemisphere geopotential at 171 hPa from the perpetual season simulations. The anticyclonic anomaly over the central Pacific (marked with an H) is somewhat stronger than in the ensemble simulations (Fig. 3a), but similarly placed. Both Southern Hemisphere wave anomalies are generated, and they are similar to those in the ensemble. The western hemisphere wave has the same path in both

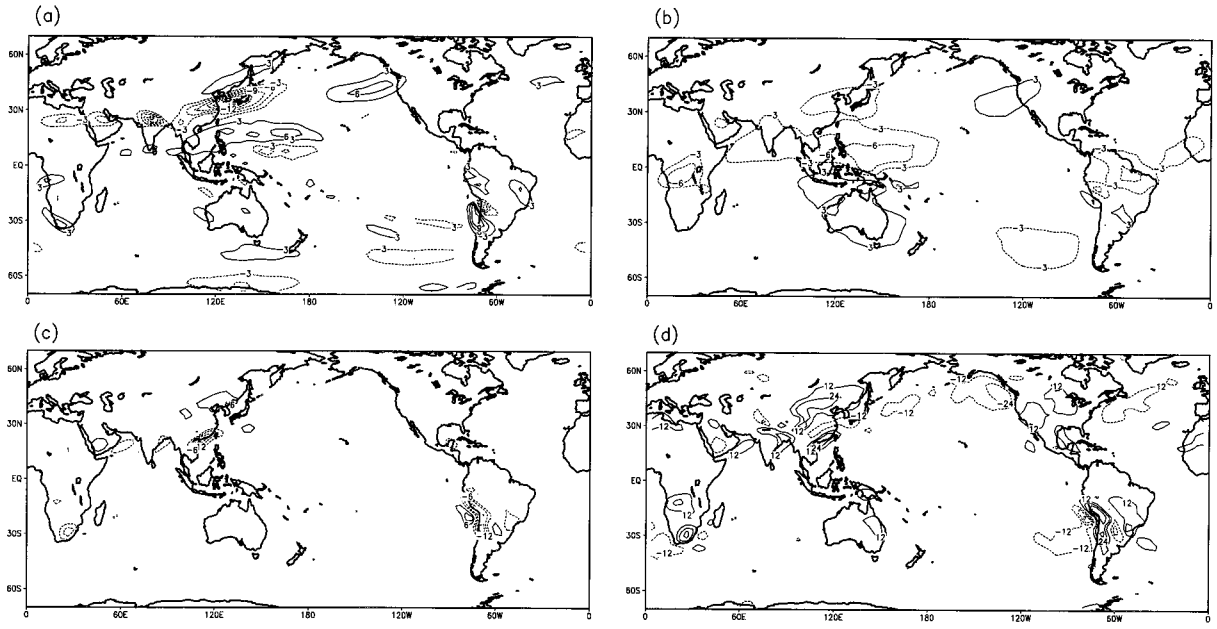

FIG. 7. Rossby wave source terms at 171 hPa in the control Dec ensemble climatology: (a) relative vorticity advection by the divergent flow, (b) planetary vorticity advection by the divergent flow, (c) stretching of relative vorticity, and (d) stretching of relative vorticity. Contour intervals are (a), (b) 3×10^{-11} s^{-2}, (c) 6×10^{-11} s^{-2}, and (d) 12×10^{-11} s^{-2}. Zero contours are not plotted.

simulation designs, but the low near 50°S and 120°W is weaker in the perpetual season case. The eastern hemisphere anomalous wave train has a path that takes it farther south in the ensemble, but the cyclonic perturbation off the southeast coast of Africa is present in both with similar strength and location. The appearance of the wave anomalies in the perpetual season simulations is further evidence, in addition to the statistical significance testing of the ensembles, that the Southern Hemisphere wave anomalies are robust responses to eastern Pacific Ocean warming.

Each of the Rossby wave source terms [Eq. (1)] was saved in the integration of the perpetual-season simulations, providing a temporal record three times the length of the ensembles and eliminating the need for approximations of the type shown in Eq. (4). The Rossby wave source analysis of the causes of the Southern Hemisphere waves in the perpetual-season integrations is in full agreement with the analysis of the ensemble simulations presented below.

Before analyzing differences in Rossby waves sources between the control and ENSO ensemble climatologies, we examine the wave sources in the control ensemble integration to provide a context for interpreting the ENSO-related differences and validation of the model. Figure 7 shows the Rossby wave source terms at 171 hPa from the control ensemble climatology for December; note the differences in the contour intervals among the four panels in Fig. 7. Relative vorticity advection by the divergent flow ($-\mathbf{v}_\chi \cdot \nabla\zeta$) and planetary vorticity advection by the divergent flow ($-v_\chi\beta$) are shown in Figs. 7a and 7b, respectively. Both tend to be largest over the tropical continents and the western Pacific warm pool where the divergence is large. Over subtropical South America, northeasterly divergent flow provides a Rossby wave source (Fig. 7a) by advecting anticyclonic relative vorticity to the southwest of the Bolivian high, which is centered at 25°S and 70°W. This term also tends to be large within the storm tracks of the winter hemisphere. The structure of the advection of planetary vorticity term (Fig. 7b) reflects the β maximum on the equator and the maxima in the divergent meridional velocity associated with the three centers of convection (equatorial Africa, South America, and the western warm pool–Maritime Continent).

Stretching of relative vorticity (Fig. 7c) acts to diminish the Rossby wave source associated with stretching of planetary vorticity (Fig. 7d; note the differences in contour intervals). Magnitudes differ by a factor of 2 or more, but structure in these two fields is strongly anticorrelated. The (mathematical) reason for this anticorrelation is that the Coriolis parameter is negative in the Southern Hemisphere while the upper-level relative vorticity is positive (anticyclonic) over Africa and South America in summer. (The anticyclonic flow over the tropical continents is part of the thermal low–upper-level high systems of the summer season.)

Figure 8 shows the total Rossby wave source anomaly due to the eastern Pacific SSTAs; this is the difference, for ENSO minus control, of the sum of the terms on the rhs of Eq. (1). In agreement with the analysis by Rasmussen and Mo (1993), the Rossby wave source anomaly is generally largest in the subtropics, or at least 10° off the equator. Positive values just east of the date

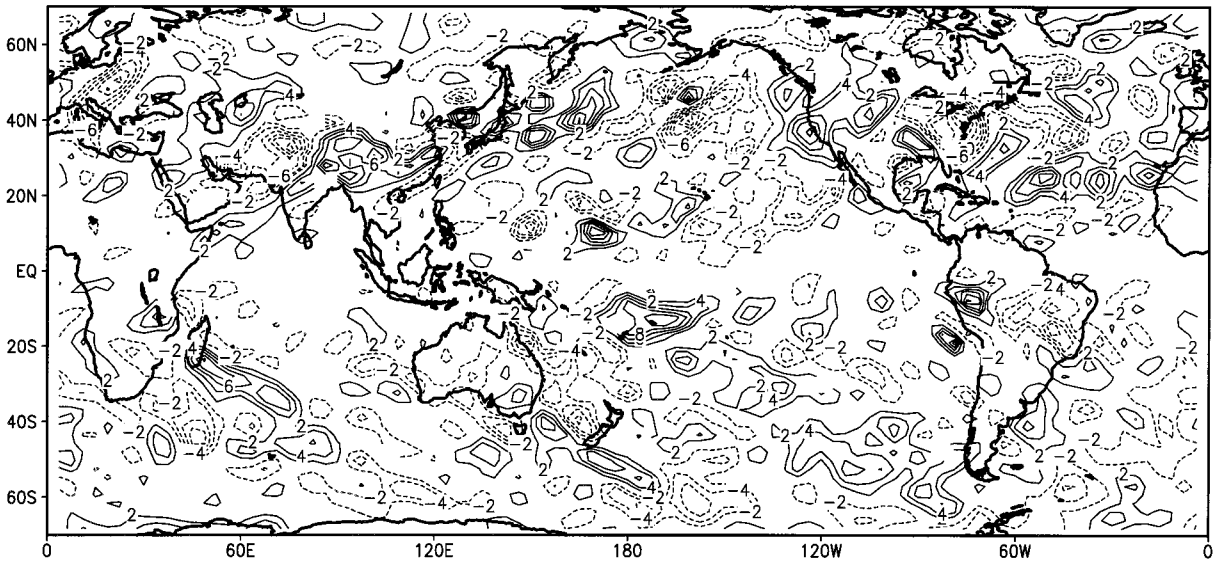

FIG. 8. Difference in 171-hPa Dec total Rossby wave source for ENSO minus control in the GCM ensemble simulations. Contour interval is 2×10^{-11} s^{-2}, and zero contours are not plotted.

line near 15°S are associated with the Southern Hemisphere anticyclone anomaly (Fig. 2). Note the generally positive values extending to the southeast of this location. These positive values are associated with the stretching of planetary vorticity term (not shown) and reflect a tendency for a northeastward shift of the South Pacific Convergence Zone (SPCZ) during warm events.

The western hemisphere wave anomaly (Figs. 2 and 3a) is not seen in the total Rossby source anomaly pattern. This is expected if the wave anomaly is a Rossby wave. We expect to see a Rossby wave source of the correct sign at the origin of the wave, but the wave pattern emanating from this source region is a free oscillation. The origin of the eastern hemisphere Rossby wave is the Southern Hemisphere anticyclone anomaly (H). The largest contributions to the total Rossby wave source in this region are the advection and stretching of planetary vorticity by the divergent flow over the central equatorial Pacific (not shown). In this sense, the western hemisphere wave is analogous to the PNA, which is thought to be associated with the Northern Hemisphere anticyclone anomaly in addition to being simply a preferred mode of variability.

The dipole pattern of the precipitation anomaly off the southeastern coast of Africa (Fig. 4) is clearly reflected in the total Rossby wave source anomaly (Fig. 8). The positive contours (anticyclonic tendency) are coincident with the positive precipitation anomalies of the ENSO perturbation, and the negative contours are coincident with the negative precipitation anomaly and the first low of the eastern hemisphere wave train (Figs. 2 and 3a). The rest of the eastern hemisphere wave train is a free Rossby mode emanating from the low off the southeast coast of Africa.

The magnitude of the Rossby wave source is consistent with the generation of a significant wave anomaly. If left in place for 1 month ($\sim 3 \times 10^6$ s), a vorticity tendency of 5×10^{-11} s^{-2} would generate a relative vorticity anomaly of about 1.5×10^{-4} s^{-1}. But cause-and-effect conclusions are still not clearly defensible. Upper-level Rossby wave sources off the southeast coast of Africa with same structure as shown in Fig. 8 would be expected as a *result* of the precipitation perturbation. However, as shown below, these Rossby wave source anomalies are not simply the result of the precipitation perturbation, and they provide the causal link between eastern Pacific SSTAs and the eastern hemisphere wave response.

Figures 9a,b show the two most important terms in the anomalous Rossby wave source anomaly near southern Africa. Stretching of relative vorticity (Fig. 9a) introduces a cyclonic (negative in the Southern Hemisphere) anomaly over southern Madagascar and out over the ocean to the southeast. As was the case for the full fields in the control case (Figs. 7c, d), the anomalous stretching of planetary vorticity (Fig. 9d) is opposite in sign to the anomalous stretching of relative vorticity, and it is 2–3 times larger. Unlike the stretching of relative vorticity term, the planetary term is in phase with the precipitation (Fig. 4) and total Rossby wave source (Fig. 8) anomalies. One expects stronger (weaker) precipitation to be associated with stronger (weaker) upper-level divergence and, therefore, a positive (negative) anomaly in the stretching of planetary vorticity.

Figure 10 shows the divergence anomaly over Africa and the adjacent oceans along with vectors of the divergent part of the flow, $\mathbf{v}_\chi$. Note that the dipole pattern of the southeast coast of Africa is still represented. The divergence field reveals structure near the equator not seen in the structure of the planetary vorticity field (Fig.

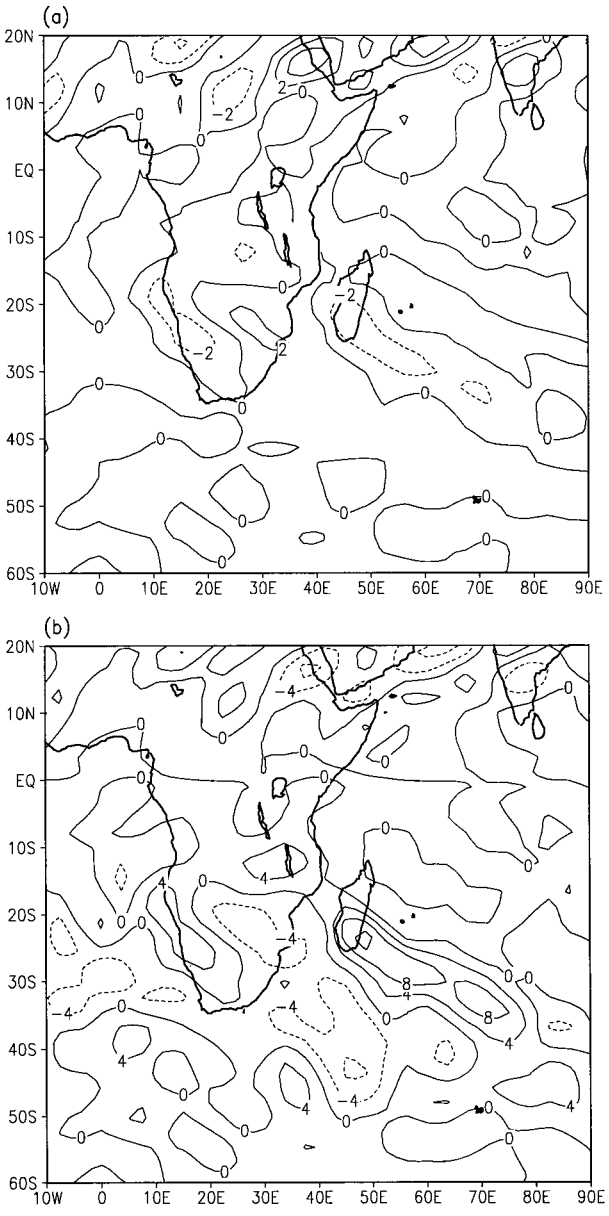

FIG. 9. Differences in the (a) stretching of relative vorticity and (b) stretching of planetary vorticity at 171 hPa due to ENSO in the GCM ensembles for Dec. Contour intervals are (a) 2×10^{-11} s^{-2} and (b) 4×10^{-11} s^{-2}.

9b) due to the smallness of the Coriolis parameter. In particular, there is a pronounced convergence anomaly very near the equator at 60°E that represents a weakening of divergence during the warm event and a decrease in precipitation over the western equatorial Indian Ocean (Fig. 4). The anomalous flow into this convergence anomaly is drawn from all directions. The flow in from the south induces upper-level divergence over Madagascar and vertical motion below, which encourages precipitation to the northeast of the SICZ's climatological position. The outflow from the enhanced precipitation provides a tendency for upper-level convergence to the southwest and, thereby, the northeastward shift of the SICZ. The convergence anomaly is coincident with the first low of the eastern hemisphere Rossby wave (cf. Figs. 9 and 2).

By associating the generation of the wave with vorticity transients, the linear model results connect the wave response with the equatorward shift of the storm track in this region. The storm track shifts equatorward in this region, behind the shift in the SICZ. The linear model analysis suggests that this provides a strong Rossby wave source through the modification of the momentum transients.

The response over the Indian Ocean is part of the adjustment of the global Walker circulation to eastern Pacific warming. Figure 11a shows the December velocity potential at 171 hPa from the ensemble simulation control. Near the equator, negative (positive) contours indicate up-branches (down-branches) of the Walker circulation. The main flow occurs across the Pacific, with rising in the warm pool–Indonesia–Indian Ocean sector, and sinking maxima over the eastern Pacific and the Atlantic–northern Africa region. Secondary up-branches are located over the Amazon and Africa, both centered near 15°S.

Figure 11b shows the December velocity potential for the average of the Decembers from the ENSO ensembles, and Fig. 11c is the difference for ENSO minus control. The largest differences occur over the Pacific between the date line and about 120°W, and represent a weakening of the main down-branch by 10% or 20%. There is also a westward shift of the Pacific Walker circulation; the zero line in Fig. 2c is west of the zero line in Fig. 2a by about 30° of longitude. Secondary maxima of upper-level anomalous divergence develop over the west coasts of equatorial South America (Ecuador and Peru) and Africa (Congo). Anomalous convergence occurs from the horn of Africa eastward to the date line, and also over the Amazon basin, reflecting the precipitation decreases in the regions (Fig. 4). Of particular note is the convergence maximum just below the Arabian Sea in the northern Indian Ocean. This is the anomaly that causes the shift of the SICZ, drying over southeastern Africa, and the generation of the eastern hemisphere wave in the model.

7. Conclusions

Ensemble GCM simulations with an idealized warm event, represented by a modest, time-dependent warming of the eastern Pacific Ocean, have been designed to study the physical mechanisms behind the global response to 20 identical idealized ENSO events in the presence of suppressed background variability. The purpose of this paper is to understand the generation of two statistically significant wave anomalies in the Southern Hemisphere. The eastern hemisphere wave anomaly is associated with a northeastward shift of the

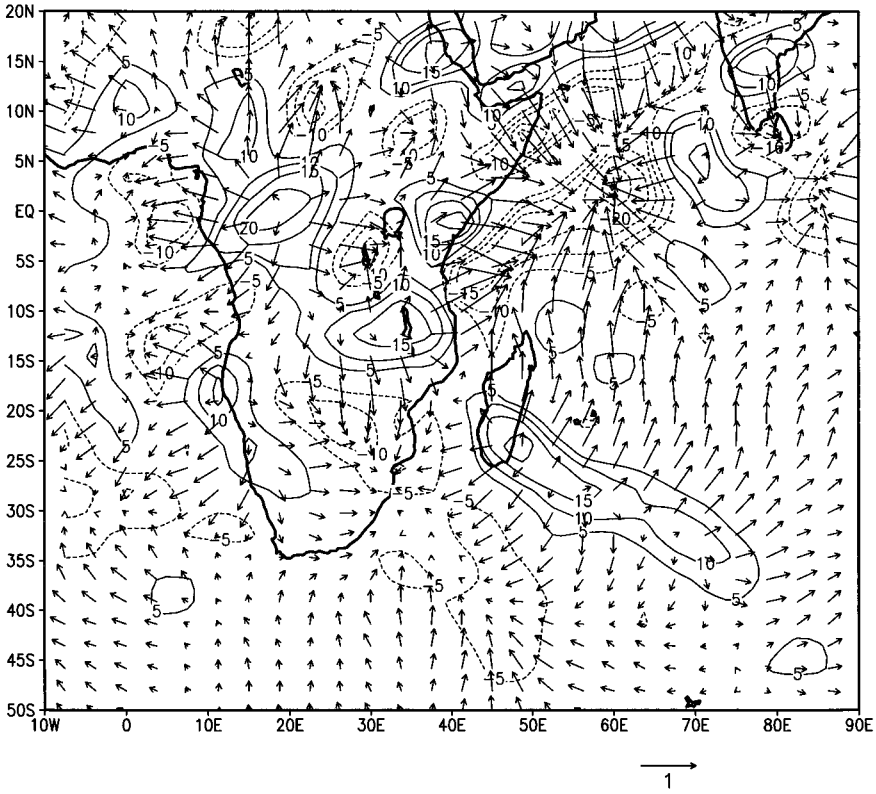

FIG. 10. Differences in 171-hPa divergence (contours) and divergent flow (vectors) due to ENSO in the GCM ensembles for Dec. Contour interval is 5×10^{-5} s^{-1}, and the vector scale is indicated in meters per second. The zero contour is not plotted.

South Indian convergence zone (SICZ) and a realistic perturbation of southern Africa rainfall, as discussed in Cook (2000). The western hemisphere wave is a result of the northeastward shift of the SPCZ during warm events.

Linear model diagnoses and Rossby wave source analyses of the ensemble GCM simulations and companion perpetual season GCM simulations are used to evaluate the causes of the Southern Hemisphere waves. The linear model, which uses zonal mean fields as a basis for linearizing, accurately reproduces both Southern Hemisphere waves, but only when vorticity transients are used to generate longitudinal structure. This linear model result is not interpreted as an indication that a modification of the vorticity transients causes the Southern Hemisphere waves since the linear model is steady state and cannot represent causality. Also, such a cause-and-effect interpretation is not physically complete, and it does not connect the wave anomalies with the eastern Pacific SSTAs. The linear model result only associates a modification of the vorticity transients with the waves, but does not indicate which way the causality runs.

The Rossby wave source analysis shows that the western hemisphere wave is a counterpart to the PNA; that is, it is the Pacific–South Atlantic signal (van Loon and Shea 1985). It emanates from the Southern Hemisphere tropical anticyclone anomaly that occurs during warm events as a result of the advection and stretching of planetary vorticity by the anomalous divergent flow over the central equatorial Pacific.

The eastern hemisphere wave is also related to the near-equatorial response of the flow to the warm event. In the model, anomalous convergence is generated over the entire northern Indian Ocean–Indonesia region as a result of the eastward shift and weakening of the Walker circulation during ENSO, with a local maximum of anomalous convergence just south of the Arabian Sea. Flow convergence into this region induces divergence to the south, encouraging upward motion in the middle troposphere, precipitation to the northeast of the usual position of the SICZ, and convergence to the southwest. The SICZ shifts to the northeast as a result, and a convergence anomaly forms off the southeast coast of Africa. This convergence anomaly, along with a modification of the vorticity flux convergence by the time-dependent flow that accompanies an equatorward shift of the Southern Hemisphere storm track behind the SICZ, provide the source for the eastern hemisphere wave.

Taken together, the linear model and the Rossby wave source analyses suggest that the fundamental cause of the wave anomalies is the adjustment of the Walker circulation to the Pacific Ocean warm event SSTAs. The

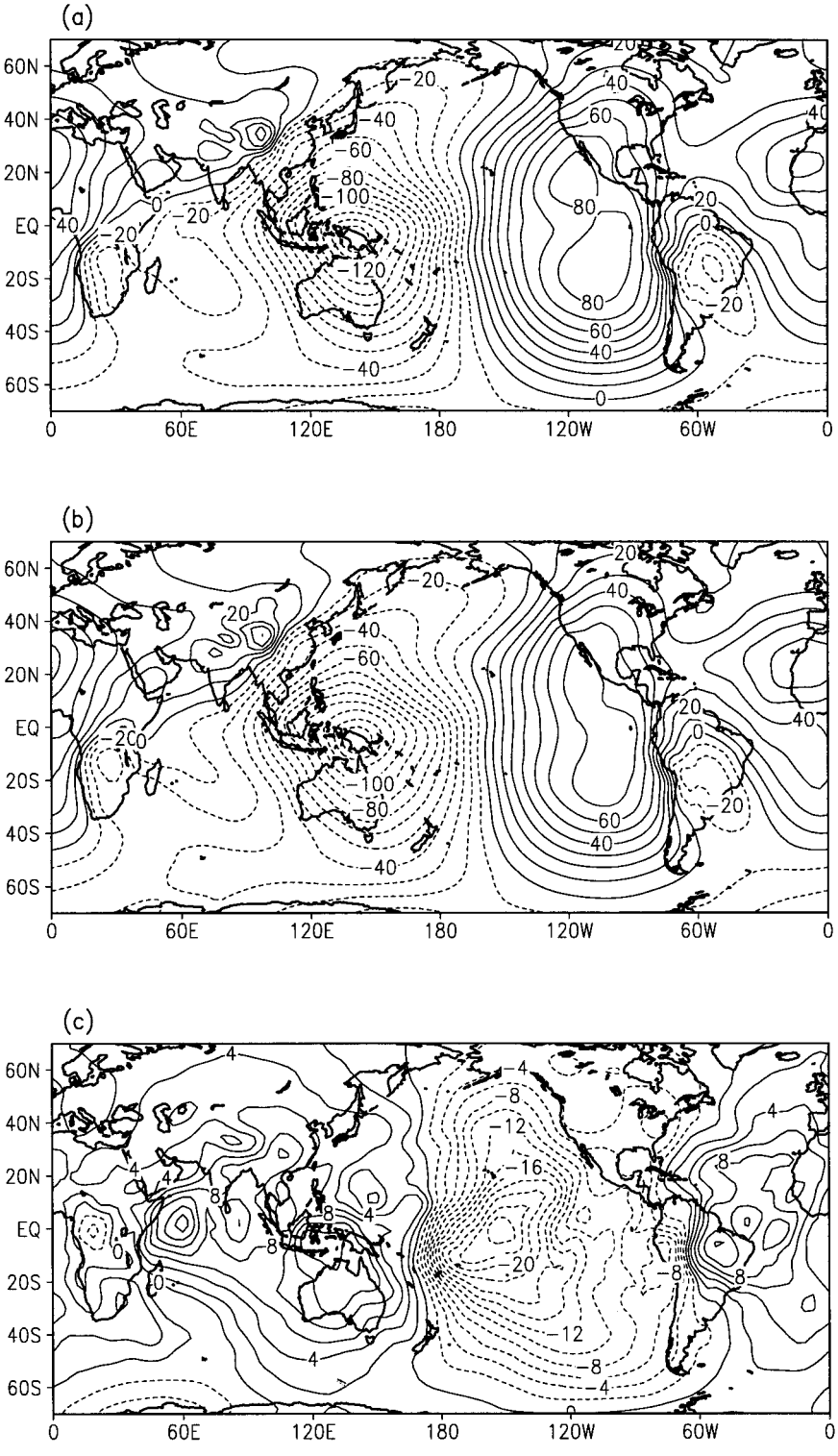

FIG. 11. Velocity potential at 171 hPa from the GCM ensemble simulations for Dec for the (a) control; (b) ENSO; and (c) difference, ENSO minus control. Contour intervals are (a), (b) 10×10^5 m^2 s^{-1} and (c) 2×10^5 m^2 s^{-1}.

linear model analysis misses the tropical origin of the waves because the model is linearized about the zonal mean flow. It does not have information about the east–west adjustment of the Walker circulation along the equator to the warm eastern Pacific SSTs; it only links the waves with the modification of the vorticity transients, providing no connection with the eastern Pacific SSTAs, which, by the design of the simulations, are the ultimate cause of the waves. Several authors [e.g., Branstator (1983); Karoly (1983); Webster and Chang (1988); Hoskins and Ambrizzi (1993)] have discussed the relevance of longitudinal structure in the background flow for determining the response to ENSO. This is a specific example, since it is the east–west anomaly in the flow in the deep tropics that leads to the subtropical–middle-latitude wave anomalies and, ultimately, the southern Africa precipitation perturbation.

This study suggests that an understanding of the details of the Walker circulation adjustment to ENSO is fundamental for understanding the global response and strengthening our prediction capabilities. Future work will be directed toward understanding the inter-ENSO variability of the tropical response, and the reasons for the strong anomaly in the Indian Ocean. A brief examination of several ENSO warm events in the reanalysis shows that the large-scale signal over the Pacific in the upper-level velocity potential field [see Fig. 3 in Trenberth et al. (1998), for example] has fairly consistent structure from one warm event to another. However, there are wide variations, even in sign, among the responses to warm events outside of the Pacific basin. The current study suggests that the response to eastern Pacific warm SSTAs in isolation is positive velocity potential anomalies over the whole Indian Ocean. It would be useful to consider how this response depends on the shape or magnitude of the ENSO forcing, and how it can be modified and/or interrupted by other sources of variability or ENSO-induced SSTAs in the Indian Ocean.

Also of interest is an exploration of the space scales involved in inducing divergence south of the equatorial convergence anomaly. What is the relevant deformation length? Are dry ENSO years over southeastern Africa always accompanied by convergence over the equatorial Indian Ocean? Does this connection explain the relationship between Indian Ocean SSTAs and southern Africa precipitation that has emerged from several statistically oriented studies (e.g., Nicholson and Kim 1997; Goddard and Graham 1999)? Perhaps the Indian Ocean SSTs are responding to the same flow anomaly as the African precipitation field, and that is why they are correlated statistically but not physically.

Of primary practical importance is to use this physical understanding of the response system to improve seasonal prediction in tropical regions, so one does not have to rely wholly on statistics to guess whether a certain region will experience ENSO-related effects during any given warm or cold event.

Acknowledgments. This research was supported by Award ATM-9815419 from NSF's Climate Dynamics Division. Thanks to John Lenters and John Chiang for their help in designing the ensemble simulations, and to Lesley Greene, John Chiang, and Brian Belcher for their help in running the GCM integrations. Brian Belcher also prepared the final versions of the figures, and John Chiang wrote the statistical analysis code for the ensembles. Comments of the anonymous reviewers are also appreciated. Graphics were generated using the Grads package developed at COLA.

REFERENCES

Aceituno, P., 1988: On the functioning of the Southern Oscillation in the South American sector. Part I: Surface climate. *Mon. Wea. Rev.*, **116,** 505–524.

Arkin, P. A., 1982: The relationship between interannual variability in the 200 mb tropical wind field and the Southern Oscillation. *Mon. Wea. Rev.*, **110,** 1393–1404.

Blackmon, M. L., J. E. Geisler, and E. J. Pitcher, 1983: A general circulation model study of January climate anomaly patterns associated with interannual variation of equatorial Pacific sea surface temperatures. *J. Atmos. Sci.*, **40,** 1410–1425.

Branstator, G. W., 1983: Horizontal energy propagation in a barotropic atmosphere with meridional and zonal structure. *J. Atmos. Sci.*, **40,** 1689–1708.

——, 1990: Low-frequency patterns induced by stationary waves. *J. Atmos. Sci.*, **47,** 629–648.

Cook, K. H., 2000: The South Indian convergence zone and interannual rainfall variability over Southern Africa. *J. Climate*, **13,** 3789–3804.

Gan, M. A., and V. B. Rao, 1991: Surface cyclogenesis over South America. *Mon. Wea. Rev.*, **119,** 1293–1302.

Geisler, J. E., M. L. Blackmon, G. T. Bates, and S. Munoz, 1985: Sensitivity of January climate response to the magnitude and position of equatorial Pacific sea surface temperature anomalies. *J. Atmos. Sci.*, **42,** 1037–1049.

Goddard, L., and N. E. Graham, 1999: Importance of the Indian Ocean for simulating rainfall anomalies over eastern and southern Africa. *J. Geophys. Res.-Atmos.*, **104,** 19 099–19 116.

Held, I. M., S. W. Lyons, and S. Nigam, 1989: Transients and the extratropical response to El Niño. *J. Atmos. Sci.*, **46,** 163–174.

Hoerling, M. P., and M.-F. Ting, 1994: Organization of extratropical transients during El Niño. *J. Climate*, **7,** 745–766.

——, ——, and A. Kumar, 1995: Zonal flow—Stationary wave relationships during El Niño: Implications for seasonal forcing. *J. Climate*, **8,** 1838–1852.

Horel, J. D., and J. M. Wallace, 1981: Planetary scale atmosphere phenomena associated with the Southern Oscillation. *Mon. Wea. Rev.*, **109,** 813–829.

Hoskins, B. J., and D. E. Karoly, 1981: The steady linear response of a spherical atmosphere to thermal and orographic forcing. *J. Atmos. Sci.*, **38,** 1179–1196.

——, and T. Ambrizzi, 1993: Rossby wave propagation on a realistic longitudinally varying flow. *J. Atmos. Sci.*, **50,** 1661–1671.

Hsu, H.-H., and S.-H. Lin, 1992: Global teleconnections in the 250-mb streamfunction field during the Northern Hemisphere winter. *Mon. Wea. Rev.*, **120,** 1169–1190.

Janowiak, J. E., 1988: An investigation of interannual rainfall variability in Africa. *J. Climate*, **1,** 240–255.

Kalnay, E., and Coauthors, 1996: The NCEP/NCAR 40-Year Reanalysis Project. *Bull. Amer. Meteor. Soc.*, **77,** 437–471.

Karoly, D. J., 1983: Rossby wave propagation in a barotropic atmosphere. *Dyn. Atmos. Oceans*, **7,** 111–125.

Kiladis, G. N., and H. F. Diaz, 1989: Global climate anomalies as-

sociated with extremes in the Southern Oscillation. *J. Climate*, **2,** 1069–1090.

Kok, C. J., and J. D. Opsteegh, 1985: On the possible causes of anomalies in the seasonal mean circulation pattern during the 1982–83 El Niño event. *J. Atmos. Sci.,* **42,** 677–694.

Latif, M., and T. P. Barnett, 1995: Interactions of the tropical oceans. *J. Climate,* **8,** 952–964.

Lau, N.-C., and E. O. Holopainen, 1984: Transient eddy forcing of the time mean flow as identified by geopotential tendencies. *J. Atmos. Sci.,* **41,** 313–328.

——, and M. J. Nath, 1990: A general circulation model study of the atmosphere response to extratropical SST anomalies observed in 1950–1979. *J. Climate,* **3,** 965–989.

Lenters, J. D., and K. H. Cook, 1999: Summertime precipitation variability over South America: Role of the large-scale circulation. *Mon. Wea. Rev.,* **127,** 409–431.

Mason, S. J., 1995: Sea-surface temperature—South African rainfall associations, 1910–1989. *Int. J. Climatol.,* **15,** 119–135.

Matthews, E., 1984: Vegetation, land use, and seasonal albedo data sets: Documentation of archived data tape. NASA Tech. Memo. 86107, 82 pp.

Mintz, Y., and G. K. Walker, 1993: Global fields of moisture and land surface evapotranspiration derived from observed precipitation and surface air temperature. *J. Appl. Meteor.,* **32,** 1305–1334.

Nicholson, S. E., and J. Kim, 1997: The relationship of the El Niño–Southern Oscillation to African rainfall. *Int. J. Climatol.,* **17,** 117–135.

Oort, A. H., and J. J. Yienger, 1996: Observed interannual variability in the Hadley circulation and its connection to ENSO. *J. Climate,* **9,** 2751–2767.

Rasmusson, E., and K.-C. Mo, 1993: Linkages between 200-mb tropical and extratropical anomalies during the 1986–1989 ENSO. *J. Climate,* **6,** 595–616.

Ringler, T. D., and K. H. Cook, 1995: Orographically induced stationary waves: Dependence on latitude. *J. Atmos. Sci.,* **52,** 2548–2560.

Rocha, A., and I. Simmonds, 1997: Interannual variability of south-eastern African summer rainfall. Part 1. Relationships with air–sea interaction processes. *Int. J. Climatol.,* **17,** 235–265.

Roeschner, E., J. M. Oberhuber, A. Bacher, M. Christoph, and I. Kirchner, 1996: ENSO variability and the atmospheric response in a global coupled atmosphere–ocean GCM. *Climate Dyn.,* **12,** 737–754.

Ropelewski, C. F., and M. S. Halpert, 1987: Global and regional scale precipitation patterns associated with El Niño–Southern Oscillation. *Mon. Wea. Rev.,* **115,** 1606–1626.

Sardeshmukh, P. D., and B. J. Hoskins, 1985: Vorticity balances in the tropics during the 1982–83 El Niño–Southern Oscillation event. *Quart. J. Roy. Meteor. Soc.,* **111,** 261–278.

——, and ——, 1988: The generation of global rotational flow by steady idealized tropical divergence. *J. Atmos. Sci.,* **45,** 1228–1251.

Shea, D. J., K. E. Trenberth, and R. W. Reynolds, 1990: A global monthly sea surface temperature climatology. NCAR Tech. Note NCAR/TN-345+STR, 167 pp. [Available from National Center for Atmospheric Research, P.O. Box 3000, Boulder, CO 80307-3000.]

Sinclair, M. R., J. A. Renwick, and J. W. Kidson, 1997: Low-frequency variability of Southern Hemisphere sea level pressure and weather system activity. *Mon. Wea. Rev.,* **125,** 2531–2543.

Ting, M.-F., and I. M. Held, 1990: The stationary wave response to a tropical SST anomaly in an idealized GCM. *J. Atmos. Sci.,* **47,** 2546–2566.

Trenberth, K. E., G. W. Branstator, D. Karoly, A. Kumar, N.-C. Lau, and C. Ropelewski, 1998: Progress during TOGA in understanding and modeling global teleconnections associated with tropical sea surface temperatures. *J. Geophys. Res.,* **103,** 14 291–14 324.

Tyson, P. D., 1986: *Climatic Change and Variability in Southern Africa.* Oxford University Press, 220 pp.

van Loon, H., and D. J. Shea, 1985: The Southern Oscillation. Part IV: The precursors south of 15°S to the extremes of the oscillation. *Mon. Wea. Rev.,* **113,** 2063–2074.

von Storch, H., and F. W. Zwiers, 1999: *Statistical Analysis in Climate Research.* Cambridge University Press, 484 pp.

Webster, P. J., and H. R. Chang, 1988: Equatorial energy accumulation and emanation regions: Impacts of a zonally varying basic state. *J. Atmos. Sci.,* **45,** 803–829.